INTERNATIONAL JOURNAL OF
NUMERICAL ANALYSIS AND MODELING
Volume 16, Number 6, Pages 964–984

ANALYSIS OF A SPECIAL IMMERSED FINITE VOLUME METHOD FOR ELLIPTIC INTERFACE PROBLEMS

KAI LIU AND QINGSONG ZOU

Abstract. In this paper, we analyze a special immersed finite volume method that is different from the classic immersed finite volume method by choosing special control volumes near the interface. Using the elementwise stiffness matrix analysis technique and the H^1-norm-equivalence between the immersed finite element space and the standard finite element space, we prove that the special finite volume method is uniformly stable independent of the location of the interface. Based on the stability, we show that our scheme converges with the optimal order $\mathcal{O}(h)$ in the H^1 space and the order $\mathcal{O}(h^{3/2})$ in the L^2 space. Numerically, we observe that our method converges with the optimal convergence rate $\mathcal{O}(h)$ under the H^1 norm and with the the optimal convergence rate $\mathcal{O}(h^2)$ under the L^2 norm all the way even with very small mesh size h, while the classic immersed finite element method is not able to maintain the optimal convergence rates (with diminished rate up to $\mathcal{O}(h^{0.82})$ for the H^1 norm error and diminished rate up to $\mathcal{O}(h^{1.1})$ for L^2-norm error), when h is getting small, as illustrated in Tables 4 and 5 of [35].

Key words. Immersed finite volume method, stability, optimal convergence rates, immersed finite element method.

1. Introduction

Interface problem is a kind of problem whose domain is typically separated by some curves or surfaces. It appears in many physical applications, such as fluid dynamics [25, 26, 9, 13, 14, 23], electromagnetic problems [4, 36, 38, 40] and materials sciences problems [31]. Many numerical methods have been applied to solve the interface problems. For standard finite element (FE) method on regular meshes, some large errors would probably happen near the interface. To eliminate these errors, the body-fitting FE method has been developed [2, 20, 53, 3, 11]. However, both of them bring the mesh generation complicated, which is particularly unadapted to the moving interface problem. To overcome the drawback, developed are a bunch of methods using a special sort of local basis functions to handle the interface based on Cartesian mesh. For example, the extended finite element method (X-FEM) [57, 51], aiming at extending the solution space via the discontinuous functions; the immersed finite element (IFE) method carrying the idea of taking the special local basis functions on an interface element [34, 10, 12, 37, 21, 32, 55, 56, 52, 8]; the enriched finite element method, based on the IFE technique with the addition of new nodal basis functions [49]. Besides, the Peskin's immersed boundary method (IBM) [41, 42], usually applied to simulate the fluid-structure interactions where the fluid is represented by an Eulerian coordinate while the structure is expressed with a Lagrangian coordinate, takes advantage of the delta function to handle the discontinuous coefficients and the jump conditions.

Unsatisfactorily however, for X-FEM, usually some penalized (or stabilized) terms have to be included in the variational formula. With regard to the IFE method, the L^2-norm convergence rate will degenerates when the mesh becomes very finer. When it comes to the enriched FE method, more degrees of freedom

Received by the editors December 2, 2018, and in final revision, June 20, 2019.
2000 *Mathematics Subject Classification.* 35R35, 49J40, 60G40.

have to be imposed near the interface. As for the IBM, it is the first order accurate method and smears the solution near the interface. In this paper, we choose the linear immersed finite element space as the trial space of finite volume (FV) method which enables us to use a uniform Cartesian mesh to solve the elliptic interface problems. There are two advantages in doing this: first, it has no need to consider mesh regeneration in a moving interface; second, many efficient solvers and numerical methods are designed for this Cartesian mesh, for example, fast Poisson solvers [1] and Particle In Cell method for plasma particle Simulation [28, 29, 50, 36].

The FV method has been widely used in numerical solutions of the partial differential equations, a key feature of which is preserving the local conservation laws. At present, the FV method is very popular in computational fluid dynamics, engineering computing, and applied in solving the hyperbolic problems [18, 24, 39, 43, 44, 45, 46, 47, 48, 5, 6]. Combining the advantage of IFE method with the local conservation property of FV mehtod, a linear immersed finite volume (IFV) method is consequently proposed [15, 16, 17, 22].

In this paper, we present a special immersed finite volume (SIFV) method on triangular mesh for solving the following elliptical interface problem. Based on the idea of the literature [54], we demonstrate the stability of the SIFV method by using the elementwise stiffness matrix analysis technique, which differs from the way presented in [16]. We construct modified control volumes for the interface element whereby the proof on stability of the SIFV method is divided into two parts. The first part is about the stability of the interface element, while the second part concerns the stability of the non-interface element. In what follows, we will mainly focus on the former, since the latter is quite natural. We adjust the position of the control vertices with parameters in order to stabilize the interface element. Afterwards, we analyze the convergence of the SIFV method. The differences of our method from the classic IFV [16] and classic IFE method are that not only it guarantees the uniform stability of our scheme in theory, but also numerically makes sure of that the convergence order in the L^2 norm is nondecreasing.

The rest of this paper is organized as follows. In Section 2, we present a special IFV scheme for elliptic equations on the triangular mesh. In Section 3, we prove the stability. In Section 4, we make a convergence analysis. In Section 5, we provide some numerical examples to verify our theories.

We close the section by some standard notations for broken Sobolev space and their associated norms. For any integer $k \geq 0$, we let:

$$\tilde{W}^{k,p}(\Omega) = \{u : u|_{\Omega^s} \in W^{k,p}(\Omega^s), s = -, +\},$$

and define the norm of $\tilde{W}^{k,p}(\Omega)$ as:

$$\|u\|^2_{k,p,\Omega} = \|u\|^2_{k,p,\Omega^-} + \|u\|_{k,p,\Omega^+},$$

and semi-norm as:

$$|u|^2_{k,p,\Omega} = |u|^2_{k,p,\Omega^-} + |u|_{k,p,\Omega^+}.$$

For convenience, we let C denote a generic positive constant which may be different at different occurrences and adopt the following notation. $A \lesssim B$ means $A \leq CB$ for some constants C that are independent of mesh sizes.

2. A special immersed finite volume element (SIFV) method

We consider the following two-dimensional elliptical interface problem on a bounded polygonal domain Ω with Lipschitz boundary $\partial\Omega$,

$$-\nabla \cdot (\beta(\mathbf{x})\nabla u(\mathbf{x})) = f(\mathbf{x}), \quad \mathbf{x} \in \Omega, \tag{1}$$

$$u(\mathbf{x}) = 0, \quad \mathbf{x} \in \partial\Omega, \tag{2}$$

where the interface Γ is a smooth curve which separates Ω into Ω^- and Ω^+, and $f \in L^2(\Omega)$, and the coefficient $\beta(\mathbf{x}) > 0$ is a piecewise constant function with $\beta(\mathbf{x}) = \beta^- > 0$ in Ω^-, and $\beta(\mathbf{x}) = \beta^+ > 0$ in Ω^+. The jump conditions across the interface Γ are:

$$[u]|_\Gamma = 0, \tag{3}$$

$$[\beta \frac{\partial u}{\partial \mathbf{n}}]|_\Gamma = 0, \tag{4}$$

where $\mathbf{n}$ is the unit normal vector of the interface Γ.

We suppose that $\mathcal{T}_h$ is a family of shape regular and conform triangulation on Ω. Assume that h is so small that the interface Γ never intersects with any edge of $\mathcal{T}_h$ more than two times. We call an element $T \in \mathcal{T}_h$ as an interface element if the interior of T intersect with the interface Γ; otherwise, we name it a non-interface element, then $\mathcal{T}_h = \mathcal{T}_h^i \cup \mathcal{T}_h^n$, where $\mathcal{T}_h^i$ be the set of interface elements and $\mathcal{T}_h^n$ be the set of non-interface elements.

Let $\mathcal{N}_h$, $\mathcal{E}_h$,$\mathring{\mathcal{E}}_h$ denote the set of all vertices of its elements, and the set of its edges, and the set of internal edges, respectively. For any internal edge e, there exist two elements T_1 and T_2 such that $T_1 \cap T_2 = e$. For a function u defined on $T_1 \cup T_2$, we define the jump $[\cdot]$ on e by:

$$[u] = u_{T_1} - u|_{T_2}.$$

We now recall linear IFE spaces in [33] and its associate IFV spaces in [16]. On each element $T \in \mathcal{T}_h$, we let

$$S_h(T) = span\{\phi_i; 1 \le i \le 3\},$$

where $\phi_i, 1 \le i \le 3$ are the standard linear nodal basis function for $T \in \mathcal{T}_h^n$; otherwise, for $T \in \mathcal{T}_h^i$, $\phi_i, 1 \le i \le 3$ are the linear IFE basis functions. To illustrate the linear IFE basic functions in interface element T as in Figure 1. We use D and E to denote its interface points. Then we define the following piecewise linear function on the interface element T,

$$\phi(x,y) = \begin{cases} \phi^+(x,y) = a^+ + b^+x + c^+y, & \forall (x,y) \in T^+, \\ \phi^-(x,y) = a^- + b^-x + c^-y, & \forall (x,y) \in T^-, \\ \phi^-(D) = \phi^+(D),\ \phi^-(E) = \phi^+(E), \\ \beta^- \nabla\phi^- \cdot \mathbf{n} = \beta^+ \nabla\phi^+ \cdot \mathbf{n}, \end{cases} \tag{5}$$

where $\mathbf{n}$ is the unit vector perpendicular to the line $\overline{DE}$. We define the IFE space over the entire solution domain Ω as follows:

$$S_h = \big\{ v : v_T \in S_h(T) \text{ and } v \text{ is continuous on } \mathcal{N}_h \big\}, \tag{6}$$

$$S_{h0} = \big\{ v : v \in S_h \text{ and } v|_{\partial\Omega} = 0 \big\}. \tag{7}$$

We then construct a dual grid $\mathcal{T}_h^*$ whose elements are called control volumes. In the finite volume methods, there are various ways to introduce control volumes. Here, for the interface element, we will construct two special control volumes. To

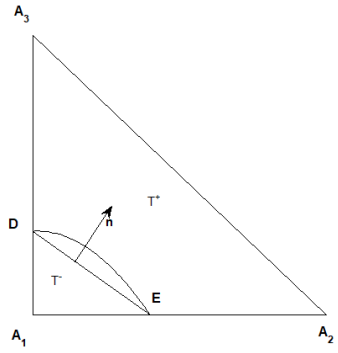

FIGURE 1. An interface element.

this end, we first assume that our mesh is sufficiently fine such that the interface elements in $\mathcal{T}_h^i$ satisfy the following hypotheses [52];

- **(H1)** The interface Γ cannot intersect an edge of any triangular element at more than two points unless the edge is part of Γ;
- **(H2)** If Γ intersects the boundary of a triangular element at two points, these intersect points must be on different edges of this element.

Then, according to the location of the intersection, there are two geometric configurations (see Fig.2) as follows:

- **Type I:** The straight line DE intersects element T at two right-angle sides.
- **Type II:** The straight line DE intersects element T at right-angle side and hypotenuse.

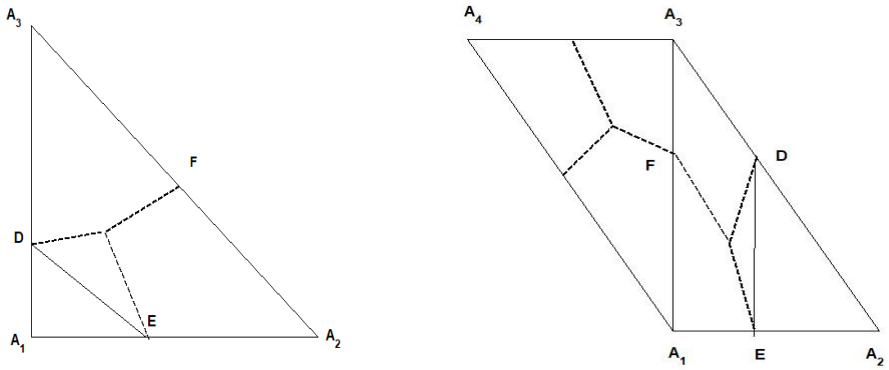

FIGURE 2. Type I, Type II geometric configurations (from left to right).

In Type I, we let D, E and midpoints of the else sides be the vertexes of control volume. In Type II, we also let D, E be the vertexes of control volume, and choose a coefficient k to automatically adjust the position of point F, which is the the vertex of the control volume at the other right-angle sides. To illustrate the idea, we construct the special control volumes in figure 2. For left side of figure 2, we have $|A_2F| = |A_3F|$. For right side of figure 2, let $\alpha_1 = \frac{|A_1E|}{|A_1A_2|}, \alpha_2 = \frac{|A_3D|}{|A_3A_2|}$. Then

point F satisfied the follow condition:

$$k = \frac{|A_1F|}{|A_1A_3|} = \frac{1+\alpha_1^2(3-2\alpha_2)-2(\alpha_2-1)^2\alpha_2-2\alpha_1((\alpha_2-3)(\alpha_2-2)\alpha_2-1)}{1-\alpha_1^3+\alpha_1^2(5-2\alpha_2)\alpha_2+\alpha_2((7-3\alpha_2)\alpha_2-4)+\alpha_1(2+\alpha_2(\alpha_2+\alpha_2^2-7))}. \tag{8}$$

Next, we introduce the control volumes from the literature [17] to construct the remaining elements.

Let S_h^* be a piecewise constant function space with respect to $\mathcal{T}_h^*$ defined by

$$S_h^* = \{\psi : \psi|_{T^*} = constant, \quad \forall T^* \in \mathcal{T}_h^*\}.$$

We call the grid $\mathcal{T}_h^*$ regular or quasi-uniform if there exists a positive constant $C > 0$ such that:

$$C^{-1}h^2 \le meas(T^*) \le Ch^2, \quad \text{for all } T^* \in \mathcal{T}_h^*.$$

From the equation (1)-(2), we know the finite volume scheme is to find a function $u_h \in S_{h0}$ that satisfies the following conservation law:

$$-\int_{\partial T^*} \beta \nabla u_h \cdot \mathbf{n} ds = \int_{T^*} f d\mathbf{x}, \quad T^* \in \mathcal{T}_h^*. \tag{9}$$

The equation (9) can be rewritten the variational form

$$a_h(u_h, v_h^*) =< f, v_h^* >, \quad \forall v_h^* \in S_h^*, \tag{10}$$

where

$$a_h(u_h, v_h^*) = -\sum_{T^* \in \mathcal{T}_h^*} v_h^* \int_{\partial T^*} \beta \nabla u_h \cdot \mathbf{n} ds, \quad \forall u_h \in S_h, v_h^* \in S_h^*,$$

$$(f, v_h^*) = \sum_{T^* \in \mathcal{T}_h^*} v_h^* \int_{T^*} f d\mathbf{x}, \quad \forall v_h^* \in S_h^*.$$

Similar to the literature [54], we define the following semi-norms:

$$|v|_{h^*} = \Big(\sum_{e \in \mathcal{E}_h^*} h_e^{-1} \int_e [v_h^*]^2 \Big)^{1/2}, \quad v_h^* \in S_h^*, \tag{11}$$

where h_e is the diameter of an edge e, and $\mathcal{E}_h^*$ is the set of interior edges of the dual mesh $\mathcal{T}_h^*$.

3. Stability

In this section, we use elementwise stiffness matrix analysis technique to prove the stability of our SIFV. The stability of the non-interface elements are naturally established, so here we only prove the stability of Type I and II of the interface elements.

In the following discussion, we exemplify approach for Type I interface element. Define $\chi_{A_i} (i = 1, 2, 3)$ are the characteristic functions on T_i^* , with T_i^* denotes by $A_i \in T_i^*$, where A_i are the vertexes of element T. Thereafter, the *element stiffness matrix* A^I of the SFIV method can be obtained by the following:

$$a_{ij} = a_\tau(\phi_i, \chi_{A_j}) = -\sum_{l=1}^{3} \int_{\partial T_i^* \cap T} (\beta \nabla \phi_i \cdot \mathbf{n}) \chi_{A_j} ds. \quad i, j = 1, 2, 3.$$

By Green's formula and the jump condition, we have :

$$-\sum_{l=1}^{3}\int_{\partial T_i^*\cap\hat{T}}(\beta\nabla\phi_i\cdot\mathbf{n})\chi_{A_j}ds=\sum_{l=1}^{3}\int_{T_i^*\cap\partial\hat{T}}(\beta\nabla\phi_i\cdot\mathbf{n})\chi_{A_j}ds.$$

For the left picture of Figure 2, we let $u_i=u_h(A_i), A_1=(0,0).A_2=(0,1), A_3=(1,0), D=(0,\alpha_2), E=(\alpha_1,0)$ and $\triangle A_1ED\in\Omega^-, \square DA_2A_3E\in\Omega^+$, then $\mathbf{n}_{DE}=(\alpha_2,\alpha_1)/|DE|$. Combining with (2.5) we have

$$\beta^-\alpha_2a^-+\beta^-\alpha_1b^-=\beta^+\alpha_2a^++\beta^+\alpha_1b^+, \tag{12}$$

$$\alpha_1a^-+c^-=\alpha_1a^++c^+,\quad \alpha_2b^-+c^-=\alpha_2b^++c^+, \tag{13}$$

$$c^-=u_1,\qquad a^++c^+=u_2,\qquad b^++c^+=u_3. \tag{14}$$

Obvious that equations (12)-(14) can be used to determine all 6 coefficients $a^\pm, b^\pm, c^\pm$. Let $b=\beta^+/\beta^-$, then we can get all the entries of A^I as follows:

$$\begin{aligned}
a^I_{11} &= -\frac{b(\alpha_1^3+\alpha_1^2\alpha_2+\alpha_1\alpha_2^2+\alpha_2^3)}{-b\alpha_1\alpha_2(\alpha_1+\alpha_2)+(\alpha_1^2(\alpha_2-1)-\alpha_2^2+\alpha_1\alpha_2^2)},\\
a^I_{12} &= \frac{b\alpha_1(\alpha_1^2+\alpha_2^2)}{-b\alpha_1\alpha_2(\alpha_1+\alpha_2)+(\alpha_1^2(\alpha_2-1)-\alpha_2^2+\alpha_1\alpha_2^2)},\\
a^I_{21} &= \frac{b\alpha_2(\alpha_1^2+\alpha_2^2)}{-b\alpha_1\alpha_2(\alpha_1+\alpha_2)+(\alpha_1^2(-1+\alpha_2)-\alpha_2^2+\alpha_1\alpha_2^2)},\\
a^I_{22} &= \frac{b(b\alpha_1\alpha_2(\alpha_1(2\alpha_2-1))-\alpha_2-(\alpha_2^2-\alpha_1\alpha_2^2+\alpha_1^2(1-\alpha_2+2\alpha_2^2)))}{2(-b\alpha_1\alpha_2(\alpha_1+\alpha_2)+(\alpha_1^2(\alpha_2-1)-\alpha_2^2+\alpha_1\alpha_2^2))}.
\end{aligned}$$

Notice that

$$\begin{aligned}
&a^I_{13}=-a^I_{11}-a^I_{12},\ a^I_{23}=-a^I_{21}-a^I_{22},\\
&a^I_{31}=-a^I_{11}-a^I_{21},\ a^I_{32}=-a^I_{12}-a^I_{22},\\
&a^I_{33}=a^I_{11}+a^I_{12}+a^I_{21}+a^I_{22}.
\end{aligned}$$

Lemma 3.1. *There exists a unique 2×2 symmetric matrix B^I such that*

$$(G^I)^tB^IG^I=\frac{A^I+(A^I)^t}{2}, \tag{15}$$

where

$$G^I=\begin{pmatrix}1&-1&0\\1&0&-1\end{pmatrix}.$$

Proof. The proof process can refer to Lemma 5 of the literature [54]. □

Lemma 3.2. *B^I is positively definite when $\alpha_1,\alpha_2\in(0,1)$.*

Proof. The eigenvalues of systematic matrix B^I can be directly calculated as follows:

$$\begin{aligned}
\lambda_1(B^I) &= -\frac{b(\alpha_1^3+\alpha_1^2\alpha_2+\alpha_1\alpha_2^2+\alpha_2^3)}{2((\alpha_1^2\alpha_2-\alpha_1^2-\alpha_2^2+\alpha_1\alpha_2^2)-b\alpha_1\alpha_2(\alpha_1+\alpha_2))}\\
\lambda_2(B^I) &= \frac{b(2b\alpha_1\alpha_2(2\alpha_1\alpha_2-\alpha_2-\alpha_1))+((\alpha_1+\alpha_2)^3-2\alpha_1^2-2\alpha_2^2-4\alpha_1^2\alpha_2^2)}{2((\alpha_1^2\alpha_2-\alpha_1^2-\alpha_2^2+\alpha_1\alpha_2^2)-b\alpha_1\alpha_2(\alpha_1+\alpha_2))}
\end{aligned}$$

In fact that $\alpha_1,\alpha_2\in(0,1)$, we get $(\alpha_1^2\alpha_2-\alpha_1^2-\alpha_2^2+\alpha_1\alpha_2^2)<0$. Thus $\lambda_1(B^I)>0$.

Defined function

$$f_1(\alpha_1,\alpha_2)=(\alpha_1+\alpha_2)^3-2\alpha_1^2-2\alpha_2^2-4\alpha_1^2\alpha_2^2.$$

Noting the function f_1 is symmetric with respect to α_1 and α_2, then we just compute the greatest value at triangle: $\triangle = \{(\alpha_1, \alpha_2)|0 < \alpha_1 < 1, \alpha_2 < \alpha_1\}$. By denoting $\alpha_2 = S\alpha_1$, we obtain that

$$f_1(\alpha_1, S) = \big((1+S)^3\alpha_1 - 2(1+S^2) - 4S^2\alpha_1^2\big)\alpha_1^2, \qquad \alpha_1, S \in (0,1).$$

In fact that $\big((1+S)^3\alpha_1 - 2(1+S^2) - 4S^2\alpha_1^2\big)|_{(0,S)} = -2(1+S^2) < 0$, $\big((1+S)^3\alpha_1 - 2(1+S^2) - 4S^2\alpha_1^2\big)|_{(1,S)} = (S-1)^3 < 0$ and $\frac{(1+S)^3}{8S^2} < 1$, it means that $f_1(\alpha_1, S) < 0$. Therefore, $\lambda_2(B^I) > 0$.

□

In Type II, stiffness matrix A^{II} contain the patch $T_1 \cup T_2 = \square A_1A_2A_3A_4$ ($T_1 = \triangle A_1A_2A_3, T_2 = \triangle A_1A_3A_4$, see Fig 2). Let $u_i = u_h(A_i)(i = 1, ..., 4), A_1 = (0,0), A_2 = (0,1), A_3 = (1,0), A_4 = (-1,1), D = (\alpha_2, 1-\alpha_2), E = (\alpha_1, 0), F = (0,k)$ and $\square A_1EDA_3A_4 \in \Omega^+, \square DEA_2 \in \Omega^-$, then $\mathbf{n}_{DE} = (1-\alpha_2, \alpha_1-\alpha_2)/|DE|$. All the entries of A^{II} as follows:

$$\begin{aligned} a_{ij}^{II} &= -\sum_{i,j=1,2,3}\int_{\partial T_i^* \cap T_1} (\beta\nabla\phi_i \cdot \mathbf{n})\chi_{A_j} ds \\ &\quad -\sum_{i,j=1,3,4}\int_{\partial T_i^* \cap T_2} (\beta\nabla\phi_i \cdot \mathbf{n})\chi_{A_j} ds. \quad i,j = 1, \cdots, 4. \end{aligned}$$

Define

$$B^{II} = \begin{pmatrix} a_{22}^{II} & \frac{a_{23}^{II}+a_{32}^{II}}{2} & \frac{a_{24}^{II}+a_{42}^{II}}{2} \\ \frac{a_{23}^{II}+a_{32}^{II}}{2} & a_{33}^{II} & \frac{a_{34}^{II}+a_{43}^{II}}{2} \\ \frac{a_{24}^{II}+a_{42}^{II}}{2} & \frac{a_{34}^{II}+a_{43}^{II}}{2} & a_{44}^{II} \end{pmatrix},$$

then all the entries of B^{II} as follows:

$$\begin{aligned} b_{11}^{II} &= \frac{b(\alpha_2-1)(1+\alpha_1^2-2\alpha_2-2\alpha_1\alpha_2+2\alpha_2^2)}{b(\alpha_1-1)(-1+\alpha_2)^2+(\alpha_1^2+\alpha_2^2+\alpha_1(1-4\alpha_2+\alpha_2^2))}, \\ b_{12}^{II} &= \frac{b(k+\alpha_2-1)(1+\alpha_1^2-2\alpha_2-2\alpha_1\alpha_2+2\alpha_2^2)}{b(1-\alpha_1)(\alpha_2-1)^2+(\alpha_1^2+\alpha_2^2+\alpha_1(1-4\alpha_2+\alpha_2^2))}, \\ b_{22}^{II} &= \frac{b(b(\alpha_1-1)(\alpha_2-1)\big(2k(1+\alpha_1-2\alpha_2)+(3+2\alpha_1)(\alpha_2-1)\big)+S_1)}{2(b(1-\alpha_1)(\alpha_2-1)^2+(\alpha_1^2+\alpha_2^2+\alpha_1(1-4\alpha_2+\alpha_2^2)))}, \\ b_{13}^{II} &= 0, \quad b_{23}^{II} = \frac{1}{4}b(2k-3), \quad b_{33}^{II} = \frac{b}{2}, \end{aligned}$$

where

$$\begin{aligned} S_1 &= \alpha_2(2k+\alpha_2-4\alpha_2^2-2)+\alpha_1^2(2\alpha_2-5-2k(\alpha_2-2)-2\alpha_2^2) \\ &\quad +\alpha_1\big((3+4k)\alpha_2^2-1-8(k-1)\alpha_2\big). \end{aligned}$$

Lemma 3.3. *B^{II} is positively definite when $\alpha_1, \alpha_2 \in (0,1)$.*

Proof. Now if $det(B^{II})$ has a positive number which depends on jump coefficient b in some connected domain containing the $b = 1$, by a simple continuity argument, we know that each eigenvalues is positive. Using the commonly used software

Mathematica, we compute that

$$
\begin{aligned}
det(B^{II}) = & \frac{-b^3\big((1-\alpha_1)^2+(\alpha_1-\alpha_2)^2\big)}{16\big(b(\alpha_1-1)(\alpha_2-1)^2-(\alpha_1^2+\alpha_2^2+\alpha_1(1-4\alpha_2+\alpha_2^2))\big)^2} \\
& \times \Big(b(\alpha_1-1)(\alpha_2-1)^2\big(4k^2(\alpha_2-1)-(3+8\alpha_1)(\alpha_2-1)+k(4-8\alpha_1+4\alpha_2)\big) \\
& + 2S_2k^2-4S_3k+S_4\Big),
\end{aligned}
$$

where

$$
\begin{aligned}
S_2 &= 1+\alpha_1^2(3-2\alpha_2)-2(\alpha_2-1)^2\alpha_2-2\alpha_1((\alpha_2-3)(\alpha_2-2)\alpha_2-1), \\
S_3 &= 1-\alpha_1^3+\alpha_1^2(5-2\alpha_2)\alpha_2+\alpha_2((7-3\alpha_2)\alpha_2-4)+\alpha_1(2+\alpha_2(\alpha_2+\alpha_2^2-7)), \\
S_4 &= 2+2\alpha_1^4-12\alpha_2+25\alpha_2^2-29\alpha_2^3+16\alpha_2^4-4\alpha_1^3(1+\alpha_2) \\
& \quad +\alpha_1(1-5\alpha_2+17\alpha_2^2-21\alpha_2^3)+\alpha_1^2(23\alpha_2-7-12\alpha_2^2+8\alpha_2^3).
\end{aligned}
$$

Then, we define some functions as follows:

$$
\begin{aligned}
(16)\quad f_2(k,\alpha_1,\alpha_2) &= 4k^2(\alpha_2-1)-(3+8\alpha_1)(\alpha_2-1)+k(4-8\alpha_1+4\alpha_2), \\
(17)\quad f_3(k,\alpha_1,\alpha_2) &= 2S_2k^2-4S_3k+S_4.
\end{aligned}
$$

Because $S_2>0, S_3>0$ and through the $Nsolve$ method of $Mathematica$ to solve the extreme values of this functions at rectangle area: $(0,1)\times(0,1)$ we can get three extreme-value points $(1/3,1),(1,1),(0.253528,0.291058)$. Then we can know that the extreme-value of the S_2-S_3 all are less than zero. It can also be directly calculated that the maximum value of the function S_2-S_3 at the boundary is also less than zero. According to the continuity of the function, we know $S_2-S_3<0$. Thus, it can be determined that the parameter $k=S_2/S_3$ belongs to the interval (0,1). Therefore, the construction of (8) in this paper is meaningful. If we want to make sure the $det(B^{II})>0$, only need to determine the function $f_2>0, f_3<0$.

First, we know that the function f_2 is a quadratic function of the variable k. Since the symmetry axis of the function on the variable k is $S_3/S_2>1$, and $f_2(0,\alpha_1,\alpha_2)=-(3+8\alpha_1)(\alpha_2-1)>0$, $f_2(1,\alpha_1,\alpha_2)=3+5\alpha_2-8\alpha_1\alpha_2>0$, thus $f_2>0$ when $k\in(0,1)$.

Second, we expand the parameter $k=S_2/S_3$ about the variable α_1,α_2, then

$$
\begin{aligned}
f_3(k,\alpha_1,\alpha_2) &= f_3(\alpha_1,\alpha_2) \\
&= \frac{S_5}{S_6}(\alpha_2-1)\big((\alpha_1-\alpha_2)^2+\alpha_1(1-\alpha_2)^2\big),
\end{aligned}
$$

where

$$
\begin{aligned}
S_5 =& 4\alpha_1^4-12\alpha_1^3+\alpha_1^2\big(8\alpha_2(3+2(\alpha_2-2)\alpha_2)-7\big)+2\alpha_2\big(\alpha_2(21+4\alpha_2(4\alpha_2-9))-5\big) \\
& -2\alpha_1\big(2+\alpha_2(1+4\alpha_2(5\alpha_2-8))\big)-3, \\
S_6 =& \alpha_1^2(2\alpha_2-3)+2\alpha_1\big((\alpha_2-3)(\alpha_2-2)\alpha_2-1\big)+2(\alpha_2-1)^2\alpha_2-1.
\end{aligned}
$$

Similar to the proof method of function f_2, the symmetry axis of the function S_6 on the variable α_1 is less than zero, and $S_6|_{\alpha_1=0}=2\alpha_2^2(\alpha_2-1)-(1-\alpha_2)^2-\alpha_2^2<0$, $S_6|_{\alpha_1=1}=2(\alpha_2-1)^2(2\alpha_2-3)<0$, we get $S_6<0$. Also, we can get the extreme-value points of S_5 by the $Nsolve$ method of $Mathematica$, it have two extreme-value points (1,1) and (0.0316798, 0.303731). By comparing the function value of S_5 at the extreme point and the maximum value of the boundary, we know $S_5<0$. So we can find the function $f_3<0$, thus $det(B^{II})>0$.

□

Let $\mathcal{E}^i$ be the set of all edges in $\mathcal{T}_h^i$ which meet the interface Γ between their vertices. Each element $e \in \mathcal{T}_h^i$ is separated into two pieces e^- and e^+ by the interface Γ such that $e^- \in \Omega^+$ and $e^+ \in \Omega^+$. We get a small positive constant $\theta << 1/2$, then we can divide region $\mathcal{T}_h^i$ into two sub-regions $\mathcal{T}_h^{ig}$ and $\mathcal{T}_h^{il}$ (for example $\theta = 10^{-4}$), where $\mathcal{T}_h^{ig}$ be the set of interface element with minimum value of $|e^-|/|e|$ and $|e^+|/|e|$ are greater than θ, and $\mathcal{T}_h^{il}$ be the set of interface element with minimum value of $|e^-|/|e|$ or $|e^+|/|e|$ is less than equal to θ. Then, there are a minimum positive value C_θ of $\lambda(B^I)$ and $\lambda(B^{II})$ at the sub-regions $\mathcal{T}_h^{ig}$.

3.1. The inf-sup condition. Now we analyze the inf-sup condition for SIFV linear form defined in (10). The finite element scheme is as follow:

$$a(u,v) := \Sigma_{T\in\mathcal{T}_h} \int_{T\in\mathcal{T}_h} \beta \nabla u \nabla v, \quad \text{for all } u, v \in \tilde{H}^1(\Omega) \cup S_h(\Omega), \tag{18}$$

and the energy norm is defined as:

$$\|u\|_h := \sqrt{a(u,v)}, \quad \text{for all } u, v \in \tilde{H}^1(\Omega) \cup S_h.$$

The discrete variational form of finite element methods of (1)-(3) is to find $u_h \in S_{h0}$ such that:

$$a(u_h, v_h) = (f, v_h), \quad \forall v_h \in S_{h0}. \tag{19}$$

Theorem 3.4. *Under the above hypotheses(***H1-H2***), the special immersed finite volume (SIFV) linear form $a_h(\cdot,\cdot)$ satisfies the inf-sup condition*

$$\inf_{u_h\in S_h(\Omega)} \sup_{v_h^*\in S_h^*(\Omega)} \frac{a_h(u_h, v_h^*)}{|u_h|_h |v_h^*|_{h^*}} \geq \alpha_\theta, \tag{20}$$

where α_θ is positive constant which may not depend on T and T^*, but depend on θ.

We begin with the H^1-norm-equivalence of the immersed finite element method and the standard finite element method. Finally we will get the proof of Theorem 3.4 in this Section.

In order to get the next theorem, we define

$$\bar{S}_h(T) = span\{\varphi_i : 1 \leq i \leq 3\}, \forall T \in \mathcal{T}_h^i,$$

where φ_i is the standard linear nodal basis function. Then define a linear mapping $\Pi : S_h(T) \to \bar{S}_h(T), \forall T \in \mathcal{T}_h^i$, by

$$\Pi\Big(\sum_{i=1}^{3} C_i \phi_i\Big) = \sum_{i=1}^{3} C_i \varphi_i, \quad \forall C_i \in \mathbb{R}.$$

In order to facilitate the calculation, we just proof the next H_1-norm-equivalence Theorem in reference element. Let $T = \Delta A_1 A_2 A_3$ with the abscissae $A_1(0,0)$, $A_2(1,0)$, and $A_3(0,1)$. The straight line DE divides T into a quadrilateral $T^+ = \square EDA_2A_3$ and a triangle $T^- = \triangle EDA_1$ (see fig3).

Now we are ready to prove the following norm-equivalence.

Lemma 3.5. *(H^1-norm-equivalence) For any $u_h|_T \in S_h(T), \forall T \in \mathcal{T}_h^i$, we have*

$$C_2 |\bar{u}_h|_{1,T} \leq |u_h|_{1,T} \leq C_1 |\bar{u}_h|_{1,T}, \tag{21}$$

where constant C_1, C_2 depending only on the coefficient $\beta(\mathbf{x}) > 0$ and independent of interface location.

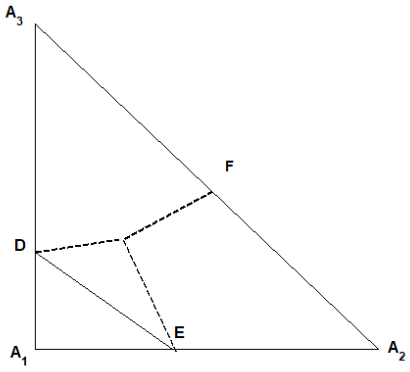

FIGURE 3. A reference interface element.

Proof. It is easy to verify that $C_{\beta,1}\int_T |\frac{\partial u_h}{\partial \mathbf{n}}|^2 \le \int_T |\frac{\partial \bar{u}_h}{\partial \mathbf{n}}|^2 \le C_{\beta,2}\int_T |\frac{\partial u_h}{\partial \mathbf{n}}|^2$ from [7]. Let

$$|u_h|^2_{1,T} = \int_T (\frac{\partial u_h}{\partial \mathbf{n}})^2 + (\frac{\partial u_h}{\partial \mathbf{t}})^2,$$

where $\mathbf{t}$ is the unit tangent vector of the line DE. Using the (12)–(14), we get

$$|\frac{\partial u_h}{\partial \mathbf{t}}|^2 = \left|\frac{u_D - u_E}{|DE|}\right|^2 = (\alpha_1^2 + \alpha_2^2)(W_1/W_2)^2,$$

where

$$W_1 = \beta^+\alpha_1\alpha_2(u_3 - u_2) + \beta^-(\alpha_2(u_3 - u_1) + \alpha_1(u_1 - u_2) + \alpha_1\alpha_2(u_2 - u_3)),$$
$$W_2 = \beta^+\alpha_1\alpha_2(\alpha_1 + \alpha_2) + \beta^-\big(\alpha_1^2(1 - \alpha_2) + \alpha_2^2(1 - \alpha_1)\big).$$

Obviously, $\beta^+\alpha_1\alpha_2(\alpha_1 + \alpha_2) > 0, (\alpha_1^2(1 - \alpha_2) + \alpha_2^2(1 - \alpha_1)) > 0$, which means that

$$W_2 < \max\{\beta^-, \beta^+\}(\alpha_1^2 + \alpha_2^2).$$

Then

$$|\frac{\partial u_h}{\partial \mathbf{t}}|^2 \le W_1^2/\big(\max\{\beta^-, \beta^+\}\big)^2(\alpha_1^2 + \alpha_2^2).$$

We notice that

$$\int_T (\frac{|u_1 - u_3|}{|P_1P_3|})^2 \le |\bar{u}_h|_1^2, \quad \int_T (\frac{|u_2 - u_1|}{|P_1P_2|})^2 \le |\bar{u}_h|_1^2, \quad \int_T (\frac{|u_2 - u_3|}{|P_2P_3|})^2 \le |\bar{u}_h|_1^2,$$

which implies

$$\int_T |\frac{\partial u_h}{\partial \mathbf{t}}|^2 \le C_{\beta,3}|\bar{u}_h|_1^2.$$

On the other hand, we consider two cases. Firstly, let $\frac{|T^-|}{|DE|^2} \leq |T^+|$, then by adding one term minus one term, we have

$$\begin{aligned}\int_T (\frac{\partial \bar{u}_h}{\partial \mathbf{t}})^2 &= \int_T \big|\frac{\bar{u}_D - \bar{u}_E}{|DE|}\big|^2 \\ &= \int_T \big(\alpha_2(u_3-u_1)+\alpha_1(u_1-u_2)\big)^2/(\alpha_1^2+\alpha_2^2) \\ &\leq C_\beta\bigg(\int_T (\frac{\partial \bar{u}_h}{\partial \mathbf{t}})^2 + \big(\alpha_1\alpha_2(u_2-u_3)\big)^2/(\alpha_1^2+\alpha_2^2)\bigg) \\ &\leq C_\beta\bigg(\int_T (\frac{\partial u_h}{\partial \mathbf{t}})^2 + |u|^2_{1,T^+}\bigg) \\ &\leq C_\beta |u|^2_{1,T}.\end{aligned}$$

Secondly, let $\frac{|T^-|}{|DE|^2} > |T^+|$, then

$$\alpha_1\alpha_2/(\alpha_1^2+\alpha_2^2) - 1 + \alpha_1\alpha_2 > 0. \tag{22}$$

Noting that (22) is symmetric with respect to α_1 and α_2, we obtain that the value range of (22) is $\alpha_1, \alpha_2 \in (\frac{1}{\sqrt{2}}, 1)$ such that $|T^-| > |T^+|$. In fact that

$$\int_T (\frac{\partial \bar{u}_h}{\partial \mathbf{t}})^2 \leq \int_T (\frac{u_2-u_1}{|P_1P_2|})^2 + (\frac{u_3-u_1}{|P_1P_3|})^2$$

Therefore,

$$\begin{aligned}\int_T (\frac{u_2-u_1}{|P_1P_2|})^2 &\lesssim h\int_{|P_1P_2|} (\frac{u_2-u_1}{|P_1P_2|})^2 \\ &\lesssim h\int_{|P_1P_2|} (\frac{\partial u_h}{\partial \mathbf{t}'})^2 \\ &\lesssim (\frac{\partial u_h|_{T^-}}{\partial \mathbf{t}'})^2 \cdot |T^-| + (\frac{\partial u_h|_{T^+}}{\partial \mathbf{t}'})^2 \cdot |T^+| \\ &\lesssim |u_h|^2_{1,T},\end{aligned}$$

where $\mathbf{t}'$ is the unit tangent vector of the vector $\overrightarrow{P_1P_2}$. Similarly, we can get $\int_T (\frac{u_2-u_1}{|P_1P_2|})^2 \lesssim |u_h|^2_{1,T}$. Combining with the above inequalities, we get $C_2|\bar{u}_h|_{1,T} \leq |u_h|_{1,T} \leq C_1|\bar{u}_h|_{1,T}$. □

For a vertex x_i of $\mathcal{N}_h$, we define $\Omega_i = \{T \in \mathcal{T}_h, x_i \in T\}$ and call it the patch of the vertex x_i. The lower bound of the sub-region $\mathcal{T}_h^{ig}$ has been given in the front of this article, and then we need to analyze sub-region $\mathcal{T}_h^{il}$.

Lemma 3.6. *When h is sufficiently small, we have*

$$\sum_{T\in\mathcal{T}_h^{il}} |\bar{v}_h|^2_{1,T} \leq \sum_{T\in\mathcal{T}_h^{n}\cup\mathcal{T}_h^{ig}} |\bar{v}_h|^2_{1,T}. \tag{23}$$

Proof. In fact, the sub-region $\mathcal{T}_h^{il}$ contain some patches. The interface Γ cut on each patch are approximate straight lines when h is sufficiently small. For convenience, we have only proved the following two cases (see Figure 4), other cases can be similarly proved.

Let $\bar{v}_h = \Sigma_{i=1}^{14} v_i\varphi_i$. we use basic functions and extended calculations directly. Then it is easy to verify that for element T_7 and $S_{T_7} = \cup_{x_i\in T_7}\Omega_i$, we have

$$|\bar{v}_h|^2_{1,T_7} \leq |\bar{v}_h|^2_{1,S_{T_7}\setminus T_7}, \quad \forall \bar{v}_h \in \bar{S}_h(T). \tag{24}$$

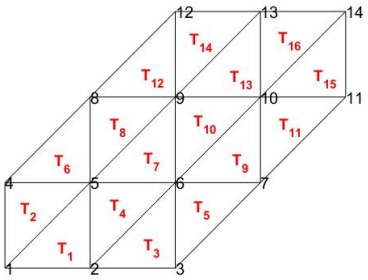

FIGURE 4. The patch of elements $T_7 \cup T_{10}$.

For element $T_7 \cup T_{10}$ and $S_{T_7 \cup T_{10}} = \cup_{x_i \in T_7 \cup T_{10}} \Omega_i$ (see Figure 4), we also have

$$|\bar{v}_h|^2_{1,T_7 \cup T_{10}} \leq |\bar{v}_h|^2_{1,S_{T_7 \cup T_{10}} \setminus T_7 \cup T_{10}}, \quad \forall \bar{v}_h \in \bar{S}_h(T). \tag{25}$$

So we know that

$$\sum_{T \in \mathcal{T}_h^{il}} |\bar{v}_h|^2_{1,T} \leq \sum_{T \in \mathcal{T}_h^n \cup \mathcal{T}_h^{ig}} |\bar{v}_h|^2_{1,T}.$$

□

Now we are ready to prove the inf-sup condition for linear IFV.

Proof. **of Theorem 3.4.** In fact, we have (semi-) norm equivalences from [54]:

$$|v_h^*|_{h^*} \simeq |\bar{v}_h|_h,$$

and $|v_h|_h \simeq |\bar{v}_h|_h$ which have been demonstrated in Theorem 3.5.

Thus if the inequality

$$a_h(v_h, v_h^*) \geq \alpha_\theta |v_h|_h^2, \tag{26}$$

holds for all $v_h \in S_h(\Omega)$, the inf-sup condition (20) holds.

Therefore

$$a_h(v_h, v_h^*) = \sum_{T \in \mathcal{T}_h^n \cup \mathcal{T}_h^{ig}} a_T(v_h, v_h^*) + \sum_{T \in \mathcal{T}_h^{il}} a_h(v_h, v_h^*).$$

From Lemma 3.2–3.3 and Lemma 3.5, we know

$$\sum_{T \in \mathcal{T}_h^n \cup \mathcal{T}_h^{ig}} a_T(v_h, v_h^*) \geq C_\theta \sum_{T \in \mathcal{T}_h^n \cup \mathcal{T}_h^{ig}} \|v_h\|^2_{1,T} \geq C_\theta \sum_{T \in \mathcal{T}_h^n \cup \mathcal{T}_h^{ig}} \|\bar{v}_h\|^2_{1,T},$$

and by Lemma 3.2–3.3, we have

$$\sum_{T \in \mathcal{T}_h^{il}} a_h(v_h, v_h^*) > 0,$$

then, combining Lemma 3.5–3.6, we get

$$\begin{aligned} a_h(v_h, v_h^*) &\geq \frac{C_\theta}{2} \Big(\sum_{T \in \mathcal{T}_h^n \cup \mathcal{T}_h^{ig}} \|\bar{v}_h\|^2_{1,T} + \sum_{T \in \mathcal{T}_h^{il}} |\bar{v}_h|^2_{1,T} \Big), \\ &\geq \alpha_\theta |v_h|^2_{1,h} \end{aligned}$$

where $\alpha_\theta = \frac{C_\theta}{2}$.

□

4. Convergence analysis

For the convenience of proof, we define a piecewise constant interpolate operator $I_h^* : S_h \to S_h^*$ such that:

$$I_h^* u(\mathbf{x}) = u(\mathbf{x}_i), \quad \forall \mathbf{x} \in T_i^*, i \in \mathcal{N}_h.$$

Lemma 4.1. *([33]) There exits a constant C such that*

$$\|u - I_h u\|_h \leq Ch\|u\|_2, \tag{27}$$

for any $u \in H^1(\Omega) \oplus S_h(\Omega)$.

Theorem 4.2. *Assume that u and u_h are the solutions of (1)-(4) and (10), respectively, then*

$$\|u - u_h\|_h \lesssim h\|u\|_2, \tag{28}$$

when h is sufficiently small.

Proof. Let $v_h = I_h u - u_h$, then by Theorem 3.4, we get

$$\begin{aligned} \|I_h u - u_h\|_h^2 &\leq a_h(I_h u - u_h, I_h^* v_h) \\ &\leq a_h(I_h u - u, I_h^* v_h) + a_h(u - u_h, I_h^* v_h) \\ &\leq a_h(I_h u - u, I_h^* v_h) \\ &\leq \|u - I_h u\|_h \|I_h u - u_h\|_h, \end{aligned}$$

and by Lemma 4.1,

$$\|u - I_h u\|_h \lesssim h\|u\|_2,$$

so that it is easy to see from triangle inequality that (28) follows. □

Lemma 4.3. *([16]) Assume that $\mathbf{M}_{lm}$ is the vertexes of control volume in the dual grid $\mathcal{T}_h^*$, then we have:*

$$a(u_h, v_h) = a_h(u_h, I_h^* v_h) + E_h(u_h, v_h), \quad u_h, v_h \in S_h, \tag{29}$$

and where:

$$E_h(u_h, v_h) = \sum_{T \cap \Gamma \neq 0} E_T(u_h, v_h),$$

and

$$\begin{aligned} E_T(u_h, v_h) = \frac{1}{2} \sum_{\overline{\mathbf{M}_{lm}} \in \partial T} \Big(&\int_{\Gamma_{lm}^l} (\beta \nabla u_h \cdot \mathbf{n})(v_h - v_l) ds + \int_{\Gamma_{lm}^m} (\beta \nabla u_h \cdot \mathbf{n})(v_h - v_m) ds \\ &+ \int_{e_{jk}} (\beta \nabla u_h \cdot \mathbf{n})(v_h - v_h(x_{jk})) ds \Big), \end{aligned} \tag{30}$$

where $l, m = i, j, k$ and point $x_{jk} \in e_{jk}$, see Figure 5.

Proof. If M_{jk} is the midpoint of edge e_{jk}, we know that

$$E_T(u_h, v_h) = \frac{1}{2} \sum_{\overline{\mathbf{M}_{lm}} \in \partial T} \Big(\int_{\Gamma_{lm}^l} (\beta \nabla u_h \cdot \mathbf{n})(v_h - v_l) ds + \int_{\Gamma_{lm}^m} (\beta \nabla u_h \cdot \mathbf{n})(v_h - v_m) ds \Big).$$

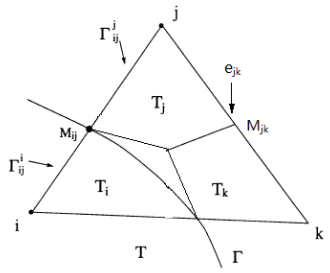

FIGURE 5. Interface of T_i^* and T_j^*.

Then, for any point $M_{jk} \in e_{jk}$, we have

$$E_T(u_h, v_h) = \frac{1}{2} \sum_{\overline{\mathbf{M}_{lm}} \in \partial T} \Big(\int_{\Gamma_{lm}^l} (\beta \nabla u_h \cdot \mathbf{n})(v_h - v_l) ds + \int_{\Gamma_{lm}^m} (\beta \nabla u_h \cdot \mathbf{n})(v_h - v_m) ds$$

$$+ \int_{e_{jk}} (\beta \nabla u_h \cdot \mathbf{n})(v_h - v_h(\mathbf{x}_{jk})) ds \Big), \tag{31}$$

where $\mathbf{x}_{jk} = \lambda_j \mathbf{x}_j + \lambda_k \mathbf{x}_k$, and $\lambda_j = \frac{|\mathbf{x}_k - M_{jk}|}{|e_{jk}|}, \lambda_k = \frac{|\mathbf{x}_j - M_{jk}|}{|e_{jk}|}$.

□

We begin with the following auxiliary problem: Let $\omega \in H_0^1(\Omega)$ be such that

$$a(\omega, v) = (u - u_h, v), \quad v \in \tilde{H}^1(\Omega) \cup S_h(\Omega), \tag{32}$$

where the bilinear form $a(\cdot, \cdot)$ is defined by (18) and u_h is the solution of (10). Clearly we have $\|\omega\|_2 \lesssim \|u - u_h\|_0$.

Theorem 4.4. *Let u be the solution of the interface problem* (1)-(4)*, and u_h be the SIFV solution of discrete variational problem* (10)*. If $u \in \tilde{H}^2(\Omega) \cap \tilde{W}^{2,\infty}(\Omega)$, and $f \in \tilde{H}^1(\Omega) \cap \tilde{W}^{1,\infty}(\Omega)$, one has*

$$\|u - u_h\|_0 \lesssim h^2(\|u\|_{2,\Omega} + |f|_{1,\Omega}) + h^{3/2}(\|u\|_{2,\infty,\Omega} + |f|_{1,\infty,\Omega}). \tag{33}$$

Proof. Let $v = u - u_h$ in (32), we have

$$\|u - u_h\|_0^2 = a(\omega, u - u_h) = a(\omega - \omega_h, u - u_h) + a(\omega_h, u - u_h). \tag{34}$$

Let $\omega_h = I_h \omega$, and by Theorem 4.2, we get

$$\begin{aligned} a(\omega - \omega_h, u - u_h) &\lesssim \|\omega - \omega_h\|_h \|u - u_h\|_h \\ &\lesssim h\|w\|_2 \|u - u_h\|_h \\ &\lesssim h^2 \|u - u_h\|_0 \|u\|_2. \end{aligned} \tag{35}$$

Next, we need to estimate the term $a(\omega_h, u - u_h)$. According to Lemma 4.3, we know

$$\begin{aligned} a(\omega_h, u - u_h) &= a(\omega_h, u) - a(\omega_h, u_h) \\ &=< f, \omega_h - I_h^* \omega_h > - E_h(u_h, \omega_h) \qquad (36) \\ &= I_1 + I_2. \qquad (37) \end{aligned}$$

We estimate the upper bound of the first term I_1,

$$\begin{aligned}
I_1 &= \sum_{T\in\mathcal{T}_h}\int_T f(\omega_h - I_h^*\omega_h)d\mathbf{x} \\
&= \sum_{T\in\mathcal{T}_h^n}\int_T f(\omega_h - I_h^*\omega_h)d\mathbf{x} + \sum_{T\in\mathcal{T}_h^i}\int_T f(\omega_h - I_h^*\omega_h)d\mathbf{x} \\
&= \sum_{T\in\mathcal{T}_h^n}\int_T (f-\bar{f})(\omega_h - I_h^*\omega_h)d\mathbf{x} + \sum_{T\in\mathcal{T}_h^i}\int_T f(\omega_h - I_h^*\omega_h)d\mathbf{x} \\
&\lesssim h^2|f|_1|\omega_h|_1 + \sum_{T\in\mathcal{T}_h^i}|f|_{1,\infty,\Omega}\int_T |\omega_h - I_h^*\omega_h|d\mathbf{x} \\
&\lesssim h^2|f|_1|\omega_h|_1 + Ch^{3/2}|f|_{1,\infty,\Omega}|\omega_h|_1,
\end{aligned}$$

and by the the proof of Lemma 4.1 in [16], and Theorem 4.2, we have

$$\begin{aligned}
&|\sum_{T\cap\Gamma\neq 0}\int_{\Gamma_{lm}^l}(\beta\nabla u_h\cdot\mathbf{n})(v_h - v_l)ds| \\
=&|\sum_{T\cap\Gamma\neq 0}\int_{\Gamma_{lm}^l}(\beta\nabla(u_h-u)\cdot\mathbf{n})(v_h - v_l)ds| \\
&+|\sum_{T\cap\Gamma\neq 0}\int_{\Gamma_{lm}^l}(\beta\nabla(u)\cdot\mathbf{n})(v_h - v_l)ds| \\
=&|\sum_{T\cap\Gamma\neq 0}\int_{\Gamma_{lm}^l}(\beta\nabla(u_h-u)\cdot\mathbf{n})(v_h - v_l)ds| \\
&+|\sum_{T\cap\Gamma\neq 0}\int_{\Gamma_{lm}^l}(\beta\nabla(u)\cdot\mathbf{n})v_h ds| \\
=&|\sum_{T\cap\Gamma\neq 0}\int_{\Gamma_{lm}^l}(\beta\nabla(u_h-u)\cdot\mathbf{n})(v_h - v_l)ds| \\
&+|\sum_{T\cap\Gamma\neq 0}\int_{\Gamma_{lm}^l}(\beta\nabla(u)\cdot\mathbf{n})(v_h - \bar{v_h})ds| \\
=&|\sum_{T\cap\Gamma\neq 0}\int_{\Gamma_{lm}^l}(\beta\nabla(u_h-u)\cdot\mathbf{n})(v_h - v_l)ds| \\
&+|\sum_{T\cap\Gamma\neq 0}\int_{\Gamma_{lm}^l}(\beta\nabla(u-Iu)\cdot\mathbf{n})(v_h - \bar{v_h})ds| \\
\lesssim& h\Big(\sum_{T\in\mathcal{T}_h^i}\|u_h\|_{1,T}^2\Big)^{1/2}\Big(\sum_{T\in\mathcal{T}_h^i}\|v_h\|_{1,T}^2\Big)^{1/2} \\
\lesssim& h\Big(\sum_{T\in\mathcal{T}_h^i}(\|u-u_h\|_{1,T}^2 \\
&+\|u\|_{1,T}^2)\Big)^{1/2}\Big(\sum_{T\in\mathcal{T}_h^i}\|v_h\|_{1,T}^2\Big)^{1/2} \\
\lesssim& \big(h^2\|u\|_{2,\Omega} + h^{3/2}\|u\|_{2,\infty,\Omega}\big)\|v_h\|_h,
\end{aligned}$$

TABLE 1. Numerical results of Classic IFVE for Example 5.1 with $\beta^- = 1, \beta^+ = 10$.

N	D^0e	$order$	D^1e	$order$	e_∞	$order$
32	1.60e-02		6.75e-01		3.66e-03	
64	4.00e-03	1.9973	3.38e-01	0.9986	1.32e-03	1.4659
128	1.00e-03	1.9988	1.69e-01	0.9991	5.29e-03	1.3241
256	2.50e-04	1.9991	8.46e-02	0.9992	2.70e-03	0.9673
512	6.27e-05	1.9986	4.24e-02	0.9982	1.21e-04	1.1557
1024	1.57e-05	1.9972	2.12e-02	0.9969	6.12e-04	0.9878
2048	3.94e-06	1.9936	1.07e-02	0.9925	3.35e-04	0.8711

TABLE 2. Numerical results of Special IFVE for Example 5.1 with $\beta^- = 1, \beta^+ = 10$.

N	D^0e	$order$	D^1e	$order$	e_∞	$order$
32	1.60e-02		6.78e-01		1.33e-03	
64	4.02e-03	1.9984	3.39e-01	0.9970	4.94e-03	1.4311
128	1.01e-03	1.9927	1.70e-01	0.9963	2.31e-03	1.0975
256	2.54e-04	1.9882	8.62e-02	0.9829	1.70e-03	0.4752
512	6.49e-05	1.9736	4.42e-02	0.9623	1.05e-04	0.6542
1024	1.66e-05	1.9635	2.30e-02	0.9450	4.63e-04	1.1893
2048	4.42e-06	1.9100	1.25e-02	0.8784	2.65e-04	0.8029

where Iu is the interpolation function of standard finite element function and $\bar{v_h}$ is the integral average of v_h,thus

$$I_2 \lesssim \big(h^2\|u\|_{2,\Omega} + h^{3/2}\|u\|_{2,\infty,\Omega}\big)\|v_h\|_h.$$

Finally, summarizing the bounds for $I_i (i = 1, 2)$ and (35) , we get

$$\|u - u_h\|_0 \lesssim h^2(\|u\|_{2,\Omega} + |f|_{1,\Omega}) + h^{3/2}(\|u\|_{2,\infty,\Omega} + |f|_{1,\infty,\Omega}).$$

□

5. Numerical Examples

In the section, the previous established convergence theory are demonstrated by three numerical examples. For the example, the computational domain are chosen as $\Omega = [-1, 1] \times [-1.1]$. The uniform triangulation of Ω is obtained by dividing Ω into N^2 sub-squares and then dividing each sub-square into two right triangles. The resulting uniform mesh size is $h = 1/N$.

For convenience, we shall adopt the following error norms in all the examples:

$$D^i e := \|u - u_h\|_{i,\Omega}, (i = 0, 1), \qquad e_\infty := max_{j\in\mathcal{N}_h}|u_I(\mathbf{x}_j) - u_h(\mathbf{x}_j)|.$$

Example 5.1, In this example, we consider the elliptic interface problem (1) with a circular interface of radius $r_0 = \frac{\pi}{6.28}$. The exact solution is

$$u(x, y) = \begin{cases} \frac{r^5}{\beta^-}, & if\ (x, y) \in \Omega^-, \\ \frac{r^5}{\beta^+} + (\frac{1}{\beta^-} - \frac{1}{\beta^+})r_0^5, & if\ (x, y) \in \Omega^+, \end{cases}$$

where $r = \sqrt{x^2 + y^2}$, $\Omega^- := \{(x, y)|x^2 + y^2 \le r^2\}$, and $\Omega^+ := \{(x, y)|x^2 + y^2 > r^2\}$.

We use two typical jump rations: $\beta^-/\beta^+ = 1/10$ and $\beta^-/\beta^+ = 1/1000$. Tables 1-4 report numerical results.

TABLE 3. Numerical results of Classic IFVE for Example 5.1 with $\beta^- = 1, \beta^+ = 1000$.

N	D^0e	$order$	D^1e	$order$	e_∞	$order$
32	1.60e-02		6.76e-01		4.89e-03	
64	4.01e-03	1.9944	3.39e-01	0.9885	2.50e-03	0.9678
128	1.01e-03	1.9930	1.69e-01	0.9853	1.63e-03	0.6176
256	2.54e-04	1.9883	8.54e-02	1.0244	1.48e-03	0.1298
512	6.44e-05	1.9814	4.32e-02	0.9213	6.74e-04	1.1433
1024	1.64e-05	1.9675	2.20e-02	0.9534	4.32e-04	0.6396
2048	4.32e-06	1.9278	1.11e-02	0.9315	2.30e-04	0.9231

TABLE 4. Numerical results of Special IFVE for Example 5.1 with $\beta^- = 1, \beta^+ = 1000$.

N	D^0e	$order$	D^1e	$order$	e_∞	$order$
32	1.60e-02		6.67e-01		8.65e-03	
64	3.99e-03	2.0038	3.39e-01	0.9971	3.52e-03	1.0979
128	9.89e-04	2.0142	1.69e-01	0.9972	1.75e-03	1.0044
256	2.45e-04	2.0135	8.54e-02	0.9920	8.64e-04	1.0207
512	5.99e-05	2.0294	4.32e-02	0.9846	4.95e-04	0.8036
1024	1.49e-05	2.0097	2.20e-02	0.9716	2.37e-04	1.0599
2048	3.82e-06	1.9649	1.14e-02	0.9440	1.23e-04	0.9466

TABLE 5. Numerical results of SIFV results for the Example 5.2.

N	D^0e	$order$	D^1e	$order$	e_∞	$order$
32	8.42e-04		5.44e-02		1.69e-03	
64	1.88e-04	2.1606	2.69e-02	1.0146	2.73e-04	2.6333
128	6.21e-05	1.5992	1.34e-02	1.0012	1.22e-05	4.4770
256	1.43e-05	2.1110	6.72e-03	0.9999	5.20e-06	1.2360
512	3.08e-06	2.2227	3.36e-03	0.9997	2.98e-06	0.8029
1024	9.36e-07	1.7200	1.68e-03	0.9990	1.93e-06	0.6263
2048	1.92e-07	2.2838	8.41e-04	1.0007	3.51e-07	2.4630

Example 5.2, In this example, we consider the elliptic interface problem (1) with a straight line edge. The exact solution is

$$u(x,y) = \begin{cases} \frac{1}{\beta^-}(x\cos(30^\circ) - y\sin(30^\circ))^2 - 0.111^2(\frac{1}{\beta^-} - \frac{1}{\beta^+}), & if\ (x,y) \in \Omega^-, \\ \frac{1}{\beta^+}(x\cos(30^\circ) - y\sin(30^\circ))^2, & if\ (x,y) \in \Omega^+, \end{cases}$$

where $\Omega^- := \{(x,y) | x\cos(30^\circ) - y\sin(30^\circ) \le 0.111\}$, and $\Omega^+ := \{(x,y) | x\cos(30) - y\sin(30) > 0.111\}$.

Numerically we test the case $\beta^-/\beta^+ = 1000$. The correspond numerical results are shown in Tables 5.

Example 5.3, In this example, we consider the elliptic interface problem (1) with a shape edge as in [19, 27, 30]. The interface given by the zero level set function $\phi(x,y) = -0.05 - y^2 + ((x-1)tan(40^\circ))^2 x$. The interface is displayed in Figure 6. The right hand function f is chosen to fit exact solution $u(x,y) = \phi(x,y)/\beta$.

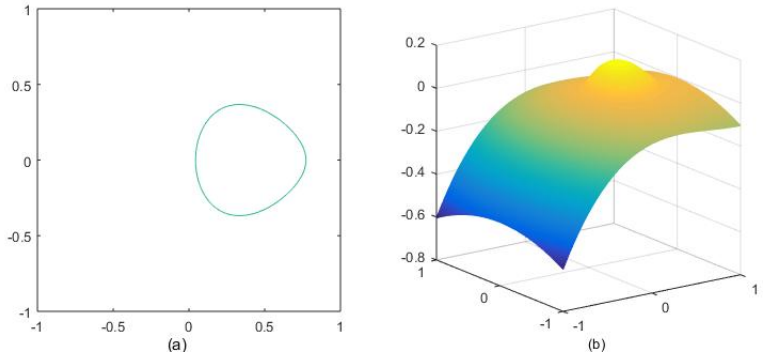

FIGURE 6. Example 5.3 with $\beta^+/\beta^- = 10$:(a) shape of interface (b) exact solution .

TABLE 6. Numerical results of SIFV results for the Example 5.3.

N	D^0e	$order$	D^1e	$order$	e_∞	$order$
32	5.54e-03		2.56e-01		6.13e-03	
64	1.38e-03	2.0007	1.28e-01	0.9785	2.14e-03	1.5144
128	3.49e-04	1.9892	6.57e-02	0.9653	1.36e-03	0.6495
256	8.88e-05	1.9742	3.56e-02	0.8840	6.85e-04	0.9981
512	2.29e-05	1.9535	2.01e-02	0.8249	3.39e-04	1.0136
1024	6.03e-06	1.9274	1.19e-02	0.7548	1.98e-04	0.7750
2048	1.60e-06	1.9543	7.00e-03	0.7700	9.31e-05	1.0915

Numerically we test the case $\beta^+/\beta^- = 10$. The correspond numerical results are shown in Tables 6.

6. Concluding remarks

We present a special immersed finite volume (SIFV) method for elliptic interface problems. We utilize the immersed finite element space to define the trial function space, selecting the piecewise constant function space as the test space, and construct some modified control volumes for the interface elements so as to ensure the stability of the SIFV method. Through such a means, the method not only retains the local conservation which is an important property of the FV method, but also is capable of handling the interface jump conditions as the IFE method does. We prove that our method achieves the optimal convergence in the energy norm and convergence rate of $\mathcal{O}(h^{3/2})$ in L^2 norm. While in practice, our numerical examples illustrate that the SFIV method owns convergence rates of $\mathcal{O}(h^2)$ in L^2 norm and $\mathcal{O}(h)$ in H^1 norm, respectively. In future, we expect to show theoretically that the convergence rate is up to $\mathcal{O}(h^2)$ with the L^2 norm for our method, and look forward to resolving the stability issue of the SIFV method taking the quadrilateral mesh.

Acknowledgments

The research was supported in part by the special project High Performance Computing of National Key Research and Development Program 2016YFB0200604, NSFC Grant 11571384, Guangdong Provincial NSF Grant 2017B030311001. The

authors are grateful to Dr. Hao Wu for many of his helps which lead a significant improvement of the paper.

References

[1] Adams J C, Swarztrauber P, Sweet R. Efficient fortran subprograms for the solution of separable elliptic partial differential equations. 1999.
[2] Babuška, Ivo. The finite element method for elliptic equations with discontinuous coefficients. Computing, 5.3 : 207-213,1970.
[3] Bramble J H, King J T. A finite element method for interface problems in domains with smooth boundaries and interfaces. Adv. Comput. Math., 6(1): 109-138, 1996.
[4] Boyd I D, Van Gilder D B, Liu X. Monte Carlo simulation of neutral xenon flows in electric propulsion devices. J. Propul. Power, 14(6): 1009-1015,1998.
[5] Cai Z, Mandel J, and McCormick S. The finite volume element method for diffusion equations on general triangulations. SIAM J. Numer. Anal., 28(2):392-402, 1991.
[6] Cai Z, McCormick S. On the accuracy of the finite volume elementmethod for diffusion equations on composite grids. SIAM J. Numer. Anal., 27(3):636-655, 1990.
[7] Cao, Waixiang, Xu Zhang, Zhiming Zhang, and Qingsong Zou. Superconvergence of immersed finite volume methods for one-dimensional inteface problems. J. Sci. Comput.. 73(2-3):543-555, 2017.
[8] Chin-Tien Wu, Zhilin Li, and Ming-Chih Lai. Adaptive mesh refinement for elliptic interface problems using the non-conforming immersed finite element method. Int. J. Numer. Anal. Model., 8(3):466-483, 2011.
[9] Chorin A J. Numerical solution of the Navier-Stokes equations. Math. Comp., 22:745-762,1968.
[10] Chou S H. An immersed linear finite element method with interface flux capturing recovery. Discrete Contin. Dyn. Syst. Ser. B, 17(7): 2343-2357. 2012.
[11] Chen Z, Zou J. Finite element methods and their convergence for elliptic and parabolic interface problems. Numer. Math., 79(2): 175-202, 1998.
[12] Chou S H, Kwak D Y, Wee K T. Optimal convergence analysis of an immersed interface finite element method. Advances in Computational Mathematics, 33(2): 149-168, 2010.
[13] Dadone A, Grossman B. Progressive optimization of inverse fluid dynamic design problems. Computers & Fluids, 29:1-32, 2000.
[14] Dadone A, Grossman B. An immersed body methodology for inviscid flows on cartesian grids. In AIAA, 2002-1059.
[15] Delanaye, M., Essers, J.A. Finite Volume Scheme with Quadratic Reconstruction on Unstructured Adaptive Meshes Applied to Turbomachinery Flows, ASME Paper 95-GT-234 presented at the International Gas Turbine and Aeroengine Congress and Exposition, Houston, June 5-8, also in the ASME Journal of Engineering for Power(1995).
[16] Ewing R E, Li Z, Lin T, et al. The immersed finite volume element methods for the elliptic interface problems. Mathematics and Computers in Simulation, 50(1):63–76, 1999.
[17] Ewing R E, Lin T, Lin Y. On the Accuracy of the Finite Volume Element Method Based on Piecewise Linear Polynomials . SIAM J. Numer. Anal., 39(6): 1865-1888, 2002.
[18] Eymard, R., Gallouet, T., Herbin, R. Finite Volume Methods, in Handbook of Numerical Analysis VII, North-Holland, Amsterdam, pp. 713-1020,2000.
[19] Guo H, Yang X. Gradient recovery for elliptic interface problem: II. Immersed finite element methods. J. Comput. Phys., 338: 606-619 , 2017.
[20] Han, Houde. "The numerical solutions of interface problems by infinite element method. Numerische Mathematik, 39.1 : 39-50, 1982.
[21] He X, Lin T, Lin Y. Immersed finite element methods for elliptic interface problems with non-homogeneous jump conditions. Int. J. Numer. Anal. Model., 8(2): 284-301, 2011.
[22] He X M, Lin T, Lin Y. A bilinear immersed finite volume element method for the diffusion equation with discontinuous coefficient. Commun. Comput. Phys., 6(1): 185,2009.
[23] Hou T Y, Wetton B T R. Second-order convergence of a projection scheme for the incompressible Navier-Stokes equations with boundaries. SIAM J. Numer. Anal., 30(3): 609-629,1993.
[24] Hyman J M, Knapp R J, Scovel J C. High order finite volume approximations of differential operators on nonuniform grids. Physica D., 60(1): 112-138, 1992.
[25] J. B. Bell, P. Colella, and H. M. Glaz. A second-order projection method for the incompressible navier-stokes equations. J. Comput. Phys, 85:257-283, 1989.
[26] J. B. Bell and D. L. Marcus. A second-order projection method for variable-density flows. J. Comput. Phys, 101:334-348, 1992.

[27] Ji H, Chen J, Li Z. A symmetric and consistent immersed finite element method for interface problems. J. Sci. Comput., 61(3): 533-557,2014.
[28] Kafafy R, Wang J. Whole ion optics gridlet simulations using a hybrid-grid immersed-finite-element particle-in-cell code. J. Propul. Power, 23(1): 59-68,2007.
[29] Kafafy R, Wang J, Lin T. A hybrid-grid immersed-finite-element particle-in-cell simulation model of ion optics plasma dynamics. Dynamics of Continuous Discrete and Impulsive Systems-Series B-Applications & Algorithms, 12: 1-16,2005.
[30] Kwak D Y, Wee K T, Chang K S. An analysis of a broken p_1-nonconforming finite element method for interface problems. SIAM J. Numer. Anal., 48(6): 2117-2134,2010,
[31] Li, Zhilin, David F. McTigue, and Jan T. Heine. A numerical method for diffusive transport with moving boundaries and discontinuous material properties. Int. J. Numer. Anal. Methods , 21.9 : 653-662,1997.
[32] Li Z, Ito K. The immersed interface method: numerical solutions of PDEs involving interfaces and irregular domains. Siam, 2006.
[33] Li Z, Lin T, Lin Y, et al. An immersed finite element space and its approximation capability. Numer. Meth. Part Differ. Equ., 20(3): 338-367, 2004.
[34] Li Z, Lin T, Wu X. New Cartesian grid methods for interface problems using the finite element formulation Numer. Math., 96(1): 61-98, 2003.
[35] Lin, Tao, Yanping Lin, and Xu Zhang. Partially penalized immersed finite element methods for elliptic interface problems. SIAM J. Numer. Anal., 53(2) : 1121-1144, 2015.
[36] Lin T, Wang J. An immersed finite element electric field solver for ion optics modeling,Proceedings of AIAA Joint Propulsion Conference, Indianapolis, IN. 2002: 2002-4263.
[37] Lin T, Zhang X. Linear and bilinear immersed finite elements for planar elasticity interface problems. J. Comput. Phys., 236(18): 4681-4699, 2012.
[38] Nakayama Y, Wilbur. Numerical simulation of ion beam optics for many-grid systems, 37th Joint Propulsion Conference and Exhibit. 2001: 3782.
[39] Ollivier-Gooch C., Altena M.V. A high-order-accurate unstructured mesh finite-volume scheme for the advection¨Cdiffusion Equation. J. Comput. Phys., 181(2), 729-752, 2002.
[40] Peng X, Ruyten W M, Friedly V J, et al. Particle simulation of ion optics and grid erosion for two-grid and three-grid systemsa. Review of scientific instruments, 65(5): 1770-1773,1994.
[41] Peskin C S. Flow patterns around heart valves, Proceedings of the Third International Conference on Numerical Methods in Fluid Mechanics. Springer, Berlin, Heidelberg, 1973: 214-221.
[42] Peskin C S. Numerical analysis of blood flow in the heart. J. Comput. Phys., 1977, 25(3): 220-252.
[43] Plexousakis, M., Zouraris, G. On the construction and analysis of high order locally conservative ?nite volume type methods for one dimensional elliptic problems. SIAM J. Numer. Anal, 42, 1226-1260, 2004.
[44] Patanker, S.V. Numerical Heat Transfer and Fluid Flow. Ser. Comput. Methods Mech. Thermal Sci. McGraw-Hill, New York ,1980.
[45] Rogiest,P.,Geuzaine,Ph.,Essers,J.A.,Delanaye,M. Implicit high-order finite volume Euler solver using multi-block structured grids. presented at the 12th AIAA CFD Conf., San Diego, June, 1995.
[46] Rogiest, P., Essers, J.A., Leonard, O. Application of High-Order Upwind Finite-Volume Scheme to 2D Cascade Flows Using a Multi-Block Approach. International Conf. on Air Breathing Engines, September 1995, ISABE Paper, 95-7057,1995.
[47] Shu C W. High-order finite difference and finite volume WENO schemes and discontinuous Galerkin methods for CFD. Int. J. Comput. Fluid Dyn., 17(2): 107-118, 2003.
[48] Sun, P., Xue, G., Wang, C., Xu, J. A combined finite element-upwind finite volume- Newton¡¯s method for liquid-feed direct methanol fuel cell simulations. Proceedings of Sixth ASME 2008 6th International Conference on Fuel Cell Science, Engineering and Technology. American Society of Mechanical Engineers, 851-864, 2008.
[49] Wang H, Chen J, Sun P, et al. A conforming enriched finite element method for elliptic interface problems. Appl. Numer. Math., 127: 1-17,2018.
[50] Wang J. The immersed finite element method for plasma particle simulations, 41st Aerospace Sciences Meeting and Exhibit. 2003: 842.
[51] Wang X, Liu W K. Extended immersed boundary method using FEM and RKPM. Comput. Meth. Appl. Mech. Eng., 193(12): 1305-1321, 2004.
[52] Xiaoming He, Tao Lin, and Yanping Lin. Approximation capability of a bilinear immersed finite element space. Numer. Meth. Part Differ. Equ., 24(5):1265-1300, 2008.

[53] Xu, Jinchao. Error estimates of the finite element method for the 2nd order elliptic equations with discontinuous coefficients. Xiangtan University, 1: 1-5, 1982.
[54] Xu J, Zou Q. Analysis of linear and quadratic simplicial finite volume methods for elliptic equations. Numer. Math., 111(3): 469-492, 2009.
[55] Yan Gong. Immersed-interface finite-element methods for elliptic and elasticity interface problems. PhD thesis, North Carolina State University, 2007.
[56] Yan Gong, Bo Li, and Zhilin Li. Immersed-interface finite-element methods for elliptic interface problems with nonhomogeneous jump conditions. SIAM J. Numer. Anal, 46(1):472-495, 2007.
[57] Zhang L, Gerstenberger A, Wang X, et al. Immersed finite element method. Computer Methods in Applied Mechanics and Engineering, 193(21): 2051-2067, 2004.

School of Data and Computer Science, Sun Yat-sen University, Guangzhou, 510006, P.R. China.
E-mail: liuk53@mail2.sysu.edu.cn

Corresponding author. School of Data and Computer Science, Guangdong Province Key Laboratory of Computational Science, Sun Yat-sen University, Guangzhou, 510006, P.R. China.
E-mail: mcszqs@mail.sysu.edu.cn